I&EC research
Industrial & Engineering Chemistry Research

pubs.acs.org/IECR

Article

Experimental and Theoretical Studies on Water-Added Thermal Processing of Model Biosyngas for Improving Hydrogen Production and Restraining Soot Formation

Svatopluk Chytil, Chao'en Li,* Woo Jin Lee,* Rune Lødeng, Anders Holmen, Edd A. Blekkan, Nick Burke, and Jim Patel*

Cite This: https://doi.org/10.1021/acs.iecr.2c01680

Read Online

ACCESS | Metrics & More | Article Recommendations | Supporting Information

ABSTRACT: The upgrading of biosyngas to convert methane into syngas is a necessary step for hydrogen production from biomass. However, this process is highly energy-demanding. In this study, a model biosyngas containing H_2, CH_4, CO, and CO_2 were thermally treated between 1200 and 1500 °C. The gas mixture, comprised of H_2 (33 vol %), CH_4 (12 vol %), CO (28 vol %), CO_2 (25 vol %), and He (2 vol %), was diluted with argon and the effect of reaction temperature (1200−1500 °C), water addition (0−44.3 mol %), and residence time (23, 46, and 76 μs in corresponding to flow rates of 1500, 2500, and 5000 mL/min at normal temperature and pressure, respectively) were studied. A possible reaction scheme for the upgrading of the model gas is proposed based on the kinetic simulation with CHEMKIN. The main reaction pathways involve dry reforming of methane and reverse water-gas shift (WGS) reactions. The kinetic simulation explained the finding that CO production was negatively influenced by the water content via the WGS reaction. The main side reaction is the methane pyrolysis reaction which causes the formation of carbon. The carbon formed in the reforming was characterized by SEM and Raman spectroscopy. SiO_2 needle-like microdomains are observed at the top of the reactor heating zone, while the central part of the heating zone was covered by carbon with a disordered, amorphous, low-density soot structure. It is proposed that the SiO_2 species formed by the chemical reaction between the reactor wall material and the reactants act as a support to anchor the carbon formed.

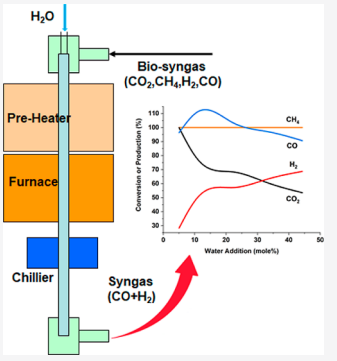

1. INTRODUCTION

To achieve net-zero emission by 2050, the energy supply needs to be diversified more significantly. In line with this aspect, energy supply from the abundant biomass, in particular, wood-based biomass from nature, should be more utilized for powering the regions with a lack of grid electricity,[1,2] which is particularly critical for the countries with a vast area. Although the production of biomethane via CO/CO_2 methanation from biosyngas (also known as producer gas) for the transportation sector is a potential direction,[3] hydrogen is considered the most promising fuel for energy and transport applications to meet the environmental and economic challenges. Hydrogen production from water splitting may be constrained by the weather conditions and the green electricity supply. Therefore, biomass has recently become a hot topic[4] due to its carbon-neutral nature and as a complement to water splitting. In the near future, this is expected to grow faster as the main processing pathway of biosyngas due to the increasing hydrogen demand.

Biosyngas is produced from the gasification of biomass at the temperature around 800−900 °C, which usually contains a mixture of versatile gaseous species including H_2, CO, CO_2, CH_4, and N_2.[5] This energy-containing gas mixture can be utilized to economically produce hydrogen, which is treated as a renewable energy carrier, and chemicals such as methane or methanol, which are directly used as transportation fuel.[6] Raw biosyngas usually contains tar compounds and other impurities such as ammonia, hydrogen sulfide and chloride, ash, and solid particles.[7] The treatment processes for removing these impurities are well developed and reviewed previously,[5,8] which thus is not the main topic in the present study. The relative concentrations of the main gaseous components in the biosyngas depends strongly on the chosen gasification agent, the type of biomass, and the process parameters used.[7,9−12] This gas mixture needs to be converted into syngas ($CO + H_2$) via the conditioning processes prior to being fed into the reaction pathway to produce hydrogen, fuel, and chemicals in the downstream. For example, the hydrogen production from biosyngas contains two steps: (1) dry- or bi-reforming to convert CH_4 into syngas ($CO + H_2$) and (2) a water-gas shift (WGS) reaction to convert CO into $CO_2 + H_2$. This study

Received: May 14, 2022
Revised: June 14, 2022
Accepted: June 15, 2022

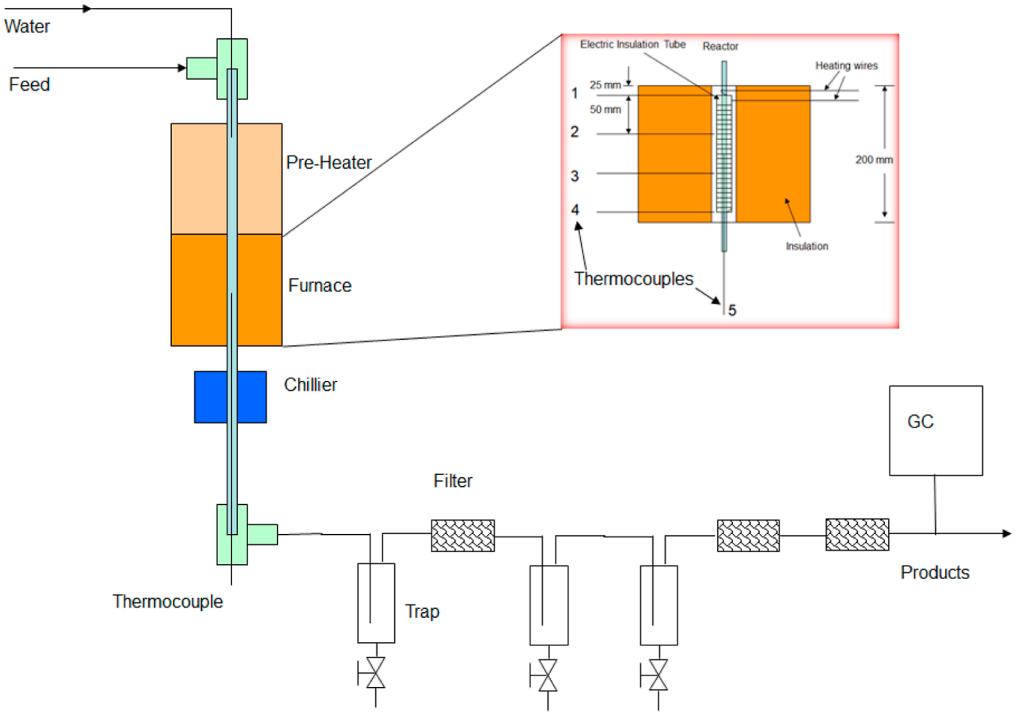

Figure 1. Configuration of the furnace and the tubular reactor.

concentrates on the first step, which using the included CO_2 converts CH_4 into syngas via dry reforming.

However, the endothermal processing of the biosyngas, mainly through dry reforming and steam reforming, makes it a highly energy-demanding process.[13] Moreover, the deposition of carbon in the form of soot is another main concern for the high-temperature reforming.[14] Soot deposition on the wall is not only a heterogenous phenomenon but also a complicated gas-phase reaction mechanism. Soot formation and the complexity of the high-temperature reaction might restrain the application of hydrogen production from biomass as an attractive process. Thus, if any improvement on the upgrading of biosyngas is made, it will greatly enhance the efficiency of the production of hydrogen from biomass. To achieve this, various efforts including bireforming or "steam biogas reforming" have been made.[15]

Upgrading of biosyngas can be performed on nickel (Ni)-based catalysts, similar to some typical processes in the petroleum industry, such as the steam reforming of methane and naphtha. However, the main drawback of using Ni-based catalysts is its relatively fast deactivation due to the carbon formation during the reforming reaction and the presence of hydrogen sulfide (H_2S) in the producer gas mixture.[16,17] Therefore, there is a considerable interest to develop optional approaches for upgrading biosyngas. The noncatalytic thermal upgrading can withstand the harsh requirement for feed gas conditions regarding the composition of feed gas and the activity of catalyst while maintaining a similar reforming performance. For example, partial oxidation in inert porous media was researched for a high-temperature biogas conversion,[18] noncatalytic reforming of biogas with steam addition under the filtration combustion mode,[19] and so on.

As reported before for catalytic reforming of biogas in the presence of syngas (CO, H_2), carbon dioxide (CO_2), C_2 species (C_2s), and water (H_2O),[7,12] the main issue for noncatalytic reforming is also the thermal decomposition of methane (CH_4) under a high temperature. The main parameters enhancing the CH_4 conversion were discussed, and different reaction schemes to predict the methane conversion[9,20] and formation pathway of polycyclic aromatic hydrocarbons (PAH) were also proposed and evaluated.[21,22]

Steam addition to the dry reforming process, as the so-called bireforming, was also well studied to have the effect of increasing the hydrogen production and restraining the carbon formation.[12,23] When conducting the experiments in the presence of a catalyst and at a lower temperature, a positive effect of added water on the methane conversion was observed.[24,25] Such observations agree with the trends predicted by thermodynamic equilibrium analysis.[25] The observed increase in methane conversion with steam/methane ratios when using an Rh catalyst[26] could also be due to the reduced carbon formation on the catalyst surface.[27] However, results obtained with Ni or Ru/ZrO_2 catalysts were different, with a zero-order dependence of added water at a higher steam addition.[24] Therefore, the presence of a catalyst makes the reaction more complex, and the noncatalytic experiments may more clearly reflect the influence of water addition.

The benefit of water addition to noncatalytic methane reforming was also realized by Valin et al.[9] and Espinoza et al.[19] Espinoza et al.[19] studied the filtration combustion of biogas/air mixtures with steam addition for biosyngas conversion to syngas and Valin et al.[9] studied the biosyngas thermal upgrading. Both found that the soot formation decreases with increasing the water content in the feed gas. However, a precise insight into the fundamental mechanisms of water-attending reactions and soot formation is still a popular research topic, and questions such as the position where the carbon deposits on the wall are still waiting for clarification.

The main purpose of the present study is to provide an insight into the behavior of gas-phase reactions, which investigates the mechanism of water addition in detail under

https://doi.org/10.1021/acs.iecr.2c01680
Ind. Eng. Chem. Res. XXXX, XXX, XXX−XXX

Table 1. Feed Compositions (mol %)

feed no.	premixture	F_0	F_5	$F_{5.5}$	$F_{11.1}$	$F_{22.1}$	$F_{33.2}$	$F_{44.3}$
H2	32.96	16.48	16.48	16.48	16.48	16.48	16.48	16.48
He	2.07	1.04	1.04	1.04	1.04	1.04	1.04	1.04
CH_4	11.99	6.00	6.00	6.00	6.00	6.00	6.00	6.00
CO	28.01	14.01	14.01	14.01	14.01	14.01	14.01	14.01
CO_2	24.97	12.49	12.49	12.49	12.49	12.49	12.49	12.49
Ar	0.00	50.00	44.96	44.47	38.93	27.87	16.80	5.74
H_2O	0.00	0.00	5.04	5.53	11.07	22.13	33.20	44.26

noncatalytic reforming conditions to reveal the effect of water addition on hydrogen production and carbon formation. This will be a valuable contribution for the design and optimization of the thermal upgrading of biosyngas. In addition to methane conversion, attention is also devoted to CO_2 conversion, which may supply more information about the influence of water addition to gas-phase chemistry. The experimental data are compared with results obtained by modeling of the gas-phase reaction using CHEMKIN Pro, and based on the simulation, a simplified reaction pathway is drawn. The contribution of the WGS reaction to gas-phase chemistry is identified via simulation. Characterization of the carbon formed in the initial phase of the reforming is also presented here, giving an insight into carbon properties and its initial growth mechanism. Moreover, when long-term (up to 4 h) experiments were performed, the periodic removal of carbon was considered.

2. EXPERIMENTAL SECTION

2.1. Furnace and Reactor. All experiments were conducted in a sintered α-SiC reactor with an internal diameter of 6 mm and length of 900 mm; however, the reaction zone is only 200 mm in length. The reactor tube was heated by an electric furnace with an upper temperature limit of 1600 °C, as shown in Figure 1. The furnace was controlled with LabVIEW program via a rewired multichannel controller (Deltech) to promptly respond the temperature change in the chamber of the furnace. There are four thermocouples marked 1 to 4 spaced 50 mm apart. LabVIEW program compares the highest temperature measured by the four thermocouples and the set value, and sends a signal to the controller which can be corrected to get the required temperature.

The preheating zone was controlled at 350 °C to ensure the evaporation of injected water. The reaction mixture was immediately cooled down by a chiller using the circulating water at 10 °C after the reactor to prevent any further reactions.

2.2. Gas Delivery and Analysis. As stated before, the composition of biosyngas varies with the origins of the biomass and the gasification conditions.[7,9−12] The premixed dry-base model biosyngas used in this study contains H_2 (32.96 vol %), CH_4 (11.99 vol %), CO (28.01 vol %), CO_2 (24.97 vol %), and He (2.07 vol %) (Coregas Pty. Ltd., Australia), where helium was used as an internal standard to calculate the conversions and productions because the sharp peak of helium comes at a very low residence time in the gas chromatograph detector and hardly has overlap with other peaks. The dry-base model gas was diluted in 50 vol % of argon when no steam was added. When steam concentration was varied from 0 to 44.26 mol %, argon was decreased to maintain a constant total flow. The total gas flow rate was varied from 1500 to 5000 mL/min at normal temperature and pressure (NTP, a temperature of 20 °C and an absolute pressure of 1 atm). The feed gas composition was listed in Table 1. It is worth noting that for the gas mixture, vol % at NTP is considered the same as mole %.

The gas flow rates were controlled by mass flow controllers (Brooks 5850E) that were regularly calibrated with a Bios Definer 220 flow meter (DryCal Tech, USA) before each run. Water was fed using a syringe pump (100 HLX, ISCO) and injected into the preheating zone which was constantly kept at 350 °C. The reaction pressure was kept at 100 kPa. When the pressure went up to a certain level (170 kPa in this experiment), mainly due to the reactor blockage caused by the carbon formation under some experimental conditions, the reaction was stopped automatically by LabVIEW program.

The effluent stream from the reactor passed through a quartz filter before entering the cooling water trap systems, as shown in Figure 1. Solid particles in the stream, if any, were removed via two porous metal filters (15 and 7 μm, Swagelok) prior to its analysis using an in-line Agilent microgas chromatograph (Agilent 490, bought from Varian, Australia), in which a 10 m long PoraPLOT U column and a 10 m long Molsieve 5 Å column were equipped with thermal conductivity detectors. Argon was used as the carrier gas. The concentration of water in the product stream was calculated based on the mass balance of oxygen.

2.3. Carbon Deposition Experiments. To understand the reaction mechanism, a set of 16 ceramic wafers (α-SiC, Ceramatec Inc., USA) were used as the substrate on which carbon was subject to be deposited. The silicon carbide wafer has the same composition and structure as the reactor which was also supplied by Ceramatec Inc. The wafers were vertically stacked in the reactor tube starting from the bottom of the reactor after cleaning using isopropanol and drying, as reported elsewhere.[28,29] The thermal upgrading for investigating carbon deposition was performed at 1500 °C, at which the total flow rate of 2500 mL/min was employed with a water content of 11.07 mol %. After exposure to this condition for the desired period (30 min), the reactor was cooled down to an ambient condition, after which the wafers were removed from the reactor for analysis (referred to $F_{11.1}T_{1500}R_{2500}t_{30}$ in Table S1d, where F refers to the water content (mol %) in the feed mixture, T represents the temperature in °C, R is the flow rate in mL/min, and t is the reaction time in minutes). The carbonaceous solids formed on the wafers were characterized by means of scanning electron microscopy (SEM, JEOL 7001F) combined with energy dispersive X-ray spectroscopy (EDX). Raman spectroscopy was performed on Renishaw Invia instrument using a laser excitation source of 514.5 nm.

3. SIMULATION METHODS

3.1. Thermodynamic Simulation. Thermodynamic equilibrium data were calculated by minimizing the Gibbs energy

https://doi.org/10.1021/acs.iecr.2c01680
Ind. Eng. Chem. Res. XXXX, XXX, XXX−XXX

using HSC CHEMISTRY 5.1 software. Activity coefficients of the species were set to unity. The conversion of feed component i ($Covt_i$) and the production of product component j ($Prod_j$) corresponding to the feed component i were calculated using the following relations[20]

$$\text{Covt}_i\,(\%) = \frac{F_{i,\text{in}} - F_{i,\text{out}}}{F_{i,\text{in}}} \times 100 \quad (1)$$

$$\text{Prod}_j\,(\%) = \frac{N_i(F_{j,\text{out}} - F_{j,\text{in}})}{N_j F_{i,\text{in}}} \times 100 \quad (2)$$

where $F_{i,\text{in}}$ and $F_{i,\text{out}}$ represent the molar flows of a compound i in the feed and in the product, $F_{j,\text{in}}$ and $F_{j,\text{out}}$ represent the molar flows of a compound j in the feed and in the product, and N_i and N_j are the stoichiometric coefficients of components i and j in the stoichiometrically balanced reaction equation, respectively.

3.2. Kinetic Simulation. The kinetic simulations were carried out using the commercial kinetic modeling software package, CHEMKIN Pro. A plug flow reactor model with fixed temperature profiles was applied. In all simulations, a constant pressure of 100 kPa was applied. A CH_4 oxidative pyrolysis mechanism developed by Skjøth-Rasmussen and Glarborg et al.,[30] which consists of 159 species and 773 fundamental chemical reactions, was applied in this modeling. This mechanism was proved more suitable for the prediction of soot precursors, especially PAHs.[9]

In such a high temperature and high flow of reactants, the actual gas temperature within the reactor is difficult to assess with reference to temperatures measured with thermocouples alone. The temperature profile can refer the measurement under a static condition or with the inert gas flow. This problem was addressed in detail by the application of computational fluid dynamic (CFD) modeling.[31] In this work, we just simply assume that the temperature profile along the reactor follows the same pattern except for the difference at the peak temperature, and the temperature profile varies linearly, with the total flow rate changing from 0 to 5 L/min.

4. EXPERIMENTAL RESULTS

4.1. Temperature Profile. A controlling program was written with LabVIEW to prevent overheating and to increase the heat efficiency. The synchronization of the output signal, the furnace current, and the temperature of the furnace during the exothermal reaction of the feed gas are shown as Figure S1. It is no surprise that the middle positions of the furnace as shown with the thermocouples 2 and 3 have higher temperatures, and the temperatures at both ends as shown with the thermocouples 1 and 4 are lower.

The temperature of the gas phase was measured by the thermocouple 5 with the tip located in the middle of the furnace in Figure 1. To test the suitability of the reactor design and to map the relationship between the gas phase and the furnace temperatures, a couple of experiments were conducted to measure the temperature profile within the reactor with and without argon flow, as shown in Figure S2. During the test, the preheater was set at 350 °C, and the furnace was controlled at 927 °C. A 1 m-long thermocouple, inserted from below, was used to determine the temperature along the reactor at 20 mm intervals. Axial positions along the reactor tube are quoted relative to the inlet (0 cm).

On inspection of the temperature profiles within the reactor it was clear that at the flow of argon the peak shifts slightly downstream and the peak temperature was lower than the reactor at static condition. The small shoulder at around 250 mm position represents the preheating zone to evaporate the injected water.

4.2. Choice of Model Biosyngas and Reaction Conditions. The relative concentrations of the species contained in biosyngas depend greatly on the gasification technology used, that is, the type of feedstock, reactor, and gasification agent. For the model gas used in this study, a composition resembling the producer gas from an air-blown biomass gasifier was selected,[7] except for the residual oxygen content, which is not safe to be premixed into the gas mixture. The relative concentrations of the species present decrease in the order of $H_2 > CO \approx CO_2 > CH_4$. Inert gas argon was used as a diluent in place of nitrogen that would otherwise originate from the air used in the gasification process. Concentrations of added water were chosen within the range that is expected when using air as a gasifying agent. The water concentrations are significantly lower than the cases when steam or steam/O_2 are used as gasifying agents. The model producer gas is, therefore, considered a relatively dry one.

CO_2 and H_2O are present in excess with respect to the possible thermal upgrading reactions of methane occurring at high temperatures (reactions R1 and R2).

$$CH_4 + CO_2 \rightarrow 2CO + 2H_2 \quad \Delta H^\circ_{298} = 247\ \text{kJ/mol} \quad (R1)$$

$$CH_4 + H_2O \rightarrow CO + 3H_2 \quad \Delta H^\circ_{298} = 206\ \text{kJ/ mol} \quad (R2)$$

For the experiments with the highest concentration of water (44.26 mol %), water is the most abundant species available for the reaction with CH_4, while for the low water concentration experiments (0 and 5 mol %), CO_2 is present in larger quantities.

4.3. Biosyngas Thermal Processing Results. Thermal upgrading experiments of the model gas were carried out in a tubular reactor. During the experiments, steam concentrations were chosen from 0 to 44.26 mol % and balanced with argon. The total gas flow at the reactor inlet was varied from 1500 to 5000 mL/min. The reaction temperature was controlled at a constant temperature from 1200 to 1500 °C. Generally, the GC analysis under each reaction condition was taken after 30 min unless for the purpose to track the production changes during the operation.

The biosyngas thermal processing results, including repeated experimental results, were summed in Table S1. Mass balances were calculated according to the GC analysis. The concentration of water in the product stream was calculated by the mass balance of oxygen. The production of species heavier than C_2, including PAH and deposited carbon, was calculated by the mas balance of carbon. In some experiments, the production of hydrogen is negative because the reversed WGS reaction occurs, which will be discussed in the section of kinetic studies.

As shown in Table S1, the processing results slightly differ with the processing time. The time-on-steam conversion for the gas mixture with a water content of 5.04 mol % reacting at 1500 °C under the flow of 2500 mL/min from 10 to 240 min

https://doi.org/10.1021/acs.iecr.2c01680
Ind. Eng. Chem. Res. XXXX, XXX, XXX−XXX

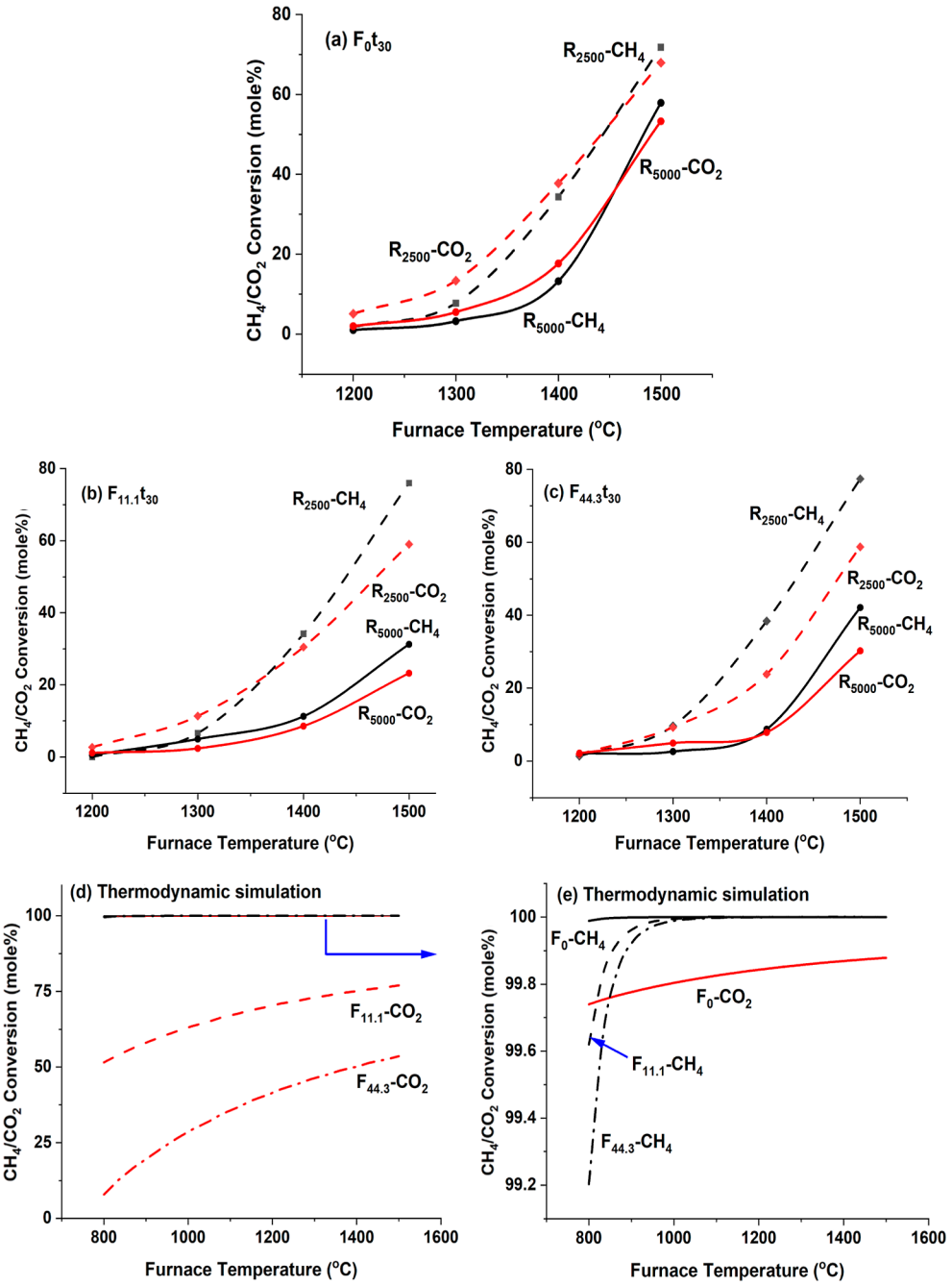

Figure 2. CH_4 and CO_2 conversions increase with the reaction temperatures for the feeds with water additions of (a) 0, (b) 11.07, and (c) 44.26 mol % at the flow rates of 5000 and 2500 mL/min, respectively; (d,e) are the thermodynamic simulation results after each water addition.

$(F_5T_{1500}R_{2500}t_{10}-F_5T_{1500}R_{2500}t_{240})$ was tracked and plotted in Figure S2. We can find that the conversion before 30 min does not reach a steady state, and the constant decline after 30 min might be caused by the carbon formation. For the purpose of investigating the optimization of reaction parameters, we simply compared the analysis data of the sample at 30 min.

5. RESULTS AND DISCUSSION

5.1. Effect of Reaction Temperature on Gas-phase Chemistry. Conversions of CO_2 and CH_4 and productions of H_2 and CO under different water additions as functions of reaction temperature are presented in Figures 2 and 3, respectively. The corresponding values based on thermodynamic equilibrium calculations are also included for comparison. Please note that the feed conversion and syngas production at thermodynamic equilibrium states are independent of residence times corresponding to different flow rates.

Inspection of Figure 2 shows that the experimental values for the CO_2 conversion under different water additions increase with the reaction temperature, following the same trend predicted by the thermodynamic calculations. Equilibrium conversion was, however, not achieved under most of the reaction conditions studied. The CO_2 conversion for the feedstock with water addition of 44.26 mol % at 1500 °C and 2500 mL/min almost reached the thermodynamic equilibrium value. Like CO_2, the methane conversion increases with the reaction temperature. The thermodynamic analysis for these

https://doi.org/10.1021/acs.iecr.2c01680
Ind. Eng. Chem. Res. XXXX, XXX, XXX−XXX

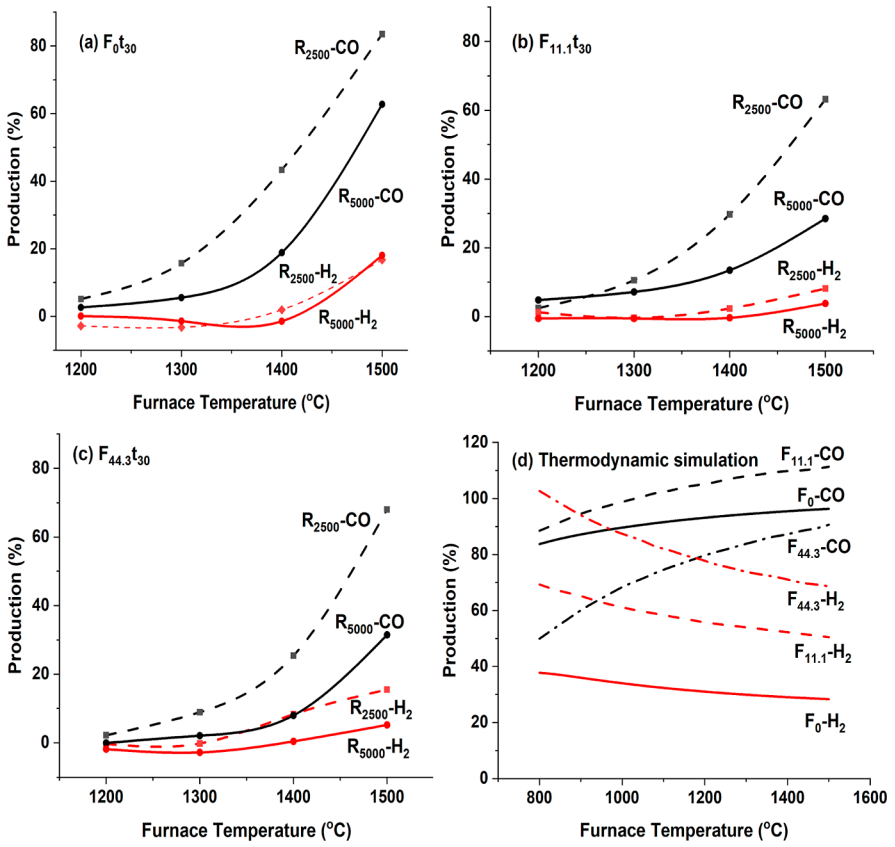

Figure 3. CO and H_2 productions increase with the reaction temperatures for the feeds with water additions of (a) 0, (b) 11.07, and (c) 44.26 mol % at the flow rates of 5000 and 2500 mL/min, respectively; (d) are the thermodynamic simulation results.

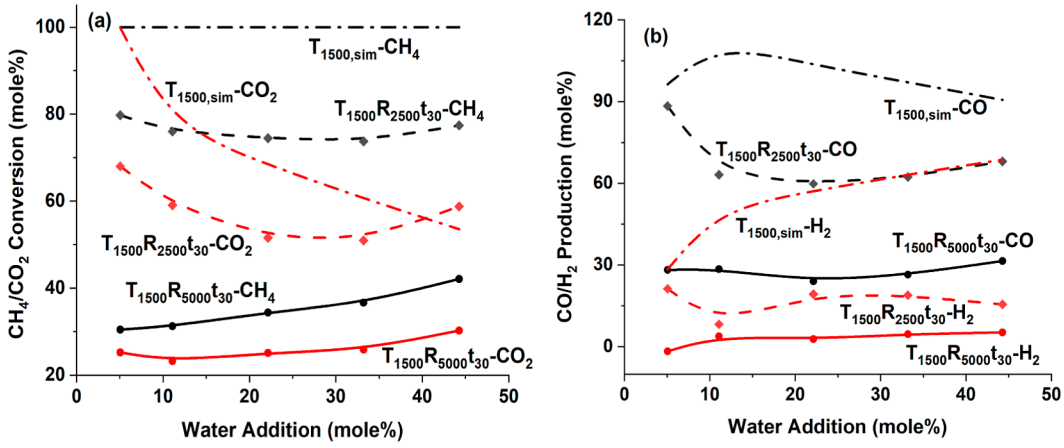

Figure 4. Thermodynamic simulation and experimental results of (a) CH_4 and CO_2 conversions and (b) CO and H_2 productions for biosyngas thermal upgrading at 1500 °C at the flow rates of 5000 and 2500 mL/min under different water additions.

sets of conditions predicts a complete CH_4 conversion regardless of the reaction temperature and the amount of water addition. The conversion also did not reach equilibrium under the experimental conditions tested, although they follow the same trend. At 1200 °C, the lowest temperature tested, the methane conversion was very low, as was the CO_2 conversion. When comparing the actual conversions of CO_2 and CH_4, both are rather close when no steam is added to the system (Figure 2a). Generally, temperature plays a more significant role than water addition in the overall conversations of methane and CO_2.

The H_2 production was found to increase with the reaction temperature and enrich the biosyngas (Figure 3). As the experiments were run at conditions where the equilibrium was not reached, the highest possible H_2 productions were not achieved. In contrast to the H_2, the CO production was significantly higher under the same condition. A maximum CO production of nearly 90% was achieved under the most favorable conditions (experiment of $F_0T_{1500}R_{2500}t_{30}$ in Figure 3a). Note that the thermodynamically predicted CO production was more than 100% under some conditions (Figure 3d). This value represents a percentage net increase relative to the CO concentration in the feed. Higher CO

https://doi.org/10.1021/acs.iecr.2c01680
Ind. Eng. Chem. Res. XXXX, XXX, XXX−XXX

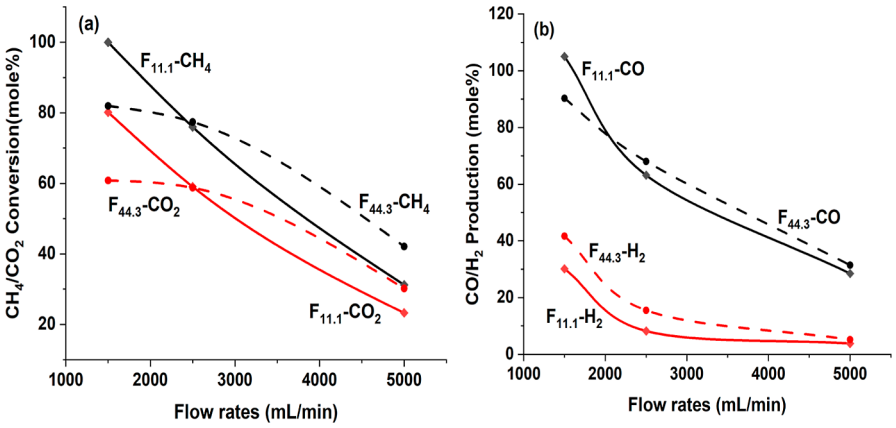

Figure 5. (a) CH_4 and CO_2 conversions and (b) CO and H_2 productions vary with the flow rates for biosyngas thermal upgrading at 1500 °C with water additions at 11.07 and 44.26 mol %, respectively.

production relative to H_2 is in accordance with the thermodynamic prediction.

Thermal upgrading reactions (reactions R1 and R2) are enhanced at elevated temperatures. However, the high temperature of over 1200 °C in thermal upgrading of the biosyngas might be a concern to the commercialization of this process. It might be compensated by increasing the recycling ratio, enlengthening the residence time, and/or introducing the catalysts as reported by this group in a separate research.[12] However, it is beyond the scope of this paper.

5.2. Effect of Water Addition on Gas-Phase Chemistry. The effect of water concentration on gas-phase chemistry can also be reflected in Figures 2 and 3. For comparison, the feed conversion and syngas production against water addition are plotted in Figure 4.

The increase of CO_2 conversion within the temperature in thermal processing was also observed experimentally by others;[9] however, to the best of our knowledge, the experiment for the effect of added water has not been fully studied except the reaction under catalysis.[12,32] As shown in Figure 4a, the CO_2 conversion at equilibrium gradually decreases with the amount of added water. The CO_2 conversion drops as expected with water addition in comparison with pure dry reforming when water addition is zero, and this trend for experiments generally agrees with the thermodynamic simulation. However, when further increasing the steam content, the CO_2 conversion goes up instead, especially when the flow rate equals 5000 mL/min. This might be because the production of the hydrogen from methane reforming promotes the reverse WGS reaction (reaction R3).

$$CO_2 + H_2 \leftrightarrow CO + H_2O \quad \Delta H^\circ_{298} = 41.2 \text{ kJ/ mol} \tag{R3}$$

For the conversion of methane, the thermodynamic analysis for these sets of conditions predicts a complete CH_4 conversion regardless of the reaction temperature and the amount of water added. The CH_4 conversion for the experiments under the flow rate of 5000 mL/min showed an increase with the water addition. However, the addition of water to the reaction system under the flow rate of 2500 mL/min has very little effect on the methane conversion. Although data presented in this study suggest that the effect of added water on the CH_4 conversion is negligible at higher conversions in comparison to the observed effect of water on the CO_2 conversion, the effect of water addition is complicated and is the competition result of a few reactions, which will be discussed in detail in the section on kinetic studies (Section 5.4).

Considering the stoichiometry of the equimolar reaction (reaction R1), it is apparent that CO_2 is mainly consumed in this methane dry reforming reaction. It is also apparent that increasing the amount of water in the reaction system has little effect on the methane conversion, whereas the CO_2 conversion is reduced. However, CO_2 conversion continues even when a significant excess of H_2O is fed into the reaction system.

Like the methane and CO_2 conversions, temperature is more important than water addition to the productions of hydrogen and CO. Clearly, the H_2 production was also influenced by the amount of added water (Figure 4b). On increasing the water concentration, the H_2 production was found to slightly increase but remain rather low. This behavior is in accordance with the thermodynamic calculations that predicted rather low H_2 productions. As the experiments were run at conditions where the equilibrium was not reached, the highest possible H_2 productions were not achieved.

The amount of added water to the reaction system has a positive influence on the extent of the methane conversion, but it also influences the CO or H_2 production and the CO_2 level through the reversible WGS reaction. The WGS reaction (the reverse reaction of reaction R3) is important for understanding the behavior of the gas mixture. The equilibrium constant K_{eq} decreases with an increasing temperature due to the exothermic nature of the reaction, and consequently, the forward WGS is thermodynamically favored at low temperatures (below 400 °C).[33] At the temperatures of this study the reverse WGS reaction is favored; therefore, the H_2 production is negative under some reaction conditions. The relatively faster reverse WGS typically occurs simultaneously with the reforming reactions and influences the product equilibration. Equilibrium production of H_2, as presented here, decreases with an increasing temperature (Figure 3d) and a decreasing water concentration in the feed (Figure 4b), presumably because of the reverse WGS. Similarly, the production of CO is negatively influenced by the water content as there is a tendency to produce H_2 via WGS. Consequently, the H_2/CO ratio of less than unity is obtained for the methane dry reforming reaction equilibrium.[25]

5.3. Effect of Residence Time on Gas-Phase Chemistry. To identify conditions that enhanced the conversions and productions, a series of experiments were performed where

https://doi.org/10.1021/acs.iecr.2c01680
Ind. Eng. Chem. Res. XXXX, XXX, XXX−XXX

Table 2. CH_4 and CO_2 Conversions (mol %) under 1500 °C Responding to Different Reactions Simulated by Kinetics

flow rate (mL/min)	5000				2500				1500			
water addition (mol %)	0.00	5.53	22.13	33.20	0.00	5.53	22.13	33.20	0.00	5.53	22.13	33.20
CH_4 conversion (mol %)	27.00	29.43	34.43	36.63	92.10	91.15	88.64	87.44	94.47	93.06	90.26	89.19
R1	0.31	0.66	1.95	2.91	7.29	12.53	27.05	35.51	14.25	22.07	40.92	52.02
R2	0.00	0.00	0.00	0.00	0.00	0.00	0.00	0.00	0.00	0.00	0.00	0.00
R44	0.08	0.08	0.07	0.06	0.01	0.01	0.01	0.01	0.01	0.02	0.02	0.02
R45	2.29	2.15	1.92	1.86	2.18	2.25	2.29	2.23	2.66	2.66	2.44	2.17
R46	22.83	24.95	28.79	30.08	79.17	73.49	57.63	48.54	74.74	66.16	45.88	34.44
R47	1.49	1.59	1.71	1.71	3.45	2.87	1.65	1.14	2.80	2.16	0.99	0.54
CO_2 conversion (mol %)	14.40	13.35	9.34	6.36	64.04	57.81	41.08	31.44	72.09	64.23	45.53	33.98
R1	0.15	0.32	0.94	1.40	3.50	6.02	12.99	17.05	6.84	10.60	19.65	24.98
R3	14.26	13.03	8.41	4.96	60.54	51.80	28.09	14.39	65.24	53.64	25.88	9.01

the total gas flow corresponding to different residence times was systematically varied. The experiments were performed with the total flows of 1500, 2500, and 5000 mL/min at the constant temperature of 1500 °C with different levels of steam. The results presented in Table S1 show an influence of the total flow and water content on the conversions and productions measured at the temperature of 1500 °C. The residence time refers to the real residence time in the reaction zone above 1100 °C; the calculation method was described in detail in the study done by Wang et al.[34] Corresponding residence times for the total flows of 5000, 2500, and 1500 mL/min are approximately 23, 46, and 76 μs, respectively. Both conversions of CH_4 and CO_2 and both productions of CO and H_2 decrease when increasing the flow rate, as shown in Figure 5, which can be explained by the change in residence time corresponding to different flow rates. This observation is also consistent with the thermodynamic predictions. However, the effect of water addition is complex, as discussed in the sections above.

In general, the experimental data collected under different flows show identical trends, an increase in conversions and productions with the increasing residence time. Water added to the reaction system also affects the conversions and productions in a consistent way for all the three flow rates used. The CO_2 conversion decreases when increasing the water content in the feed, while the CH_4 conversion remains rather unaffected by the increasing water content. Water has a slightly positive effect on H_2 production, but CO production decreases with an increasing water amount in the system.

5.4. Kinetic Studies. As discussed above, the effect of water addition is a competition result of a series of reactions. To better understand the thermal processing of biosyngas, kinetic studies were performed using CHEMKIN Pro and the mechanism developed by Skjøth-Rasmussen and Glarborg et al.[30] The main fundamental reactions attended by the components inside the feedstock were summed in Table S2 from reactions 4−43. The reaction rates in centimeter−mole−seconds for the feedstock having water addition of 0 and 22.1 mol % under 1500 °C and 2500 mL/min of flow rates at the positions of the top (36.1 cm from the inlet of the reactor, marked as $L_{36.1}$) and middle (52.0 cm from the inlet of the reactor, marked as $L_{52.0}$) of the heating zone are plotted in Figure S4.

There is no surprise for the reactions with CH_4, CO_2, and CO. The reaction of methane is dominated by reaction R4, and the reactions of CO_2 and CO are dominated by reaction R11, regardless of water addition and position along the reactor tube (reflecting different temperature zones).

$$CH_4 + H \rightarrow CH_3 + H_2 \quad \text{(R4)}$$

$$CO_2 + H \rightarrow CO + OH \quad \text{(R11)}$$

Generally, water is produced mainly via reactions R6 and R14, corresponding to dry reforming and reverse WGS reaction, respectively

$$CH_4 + OH \rightarrow CH_3 + H_2O \quad \text{(R6)}$$

$$H_2 + OH \rightarrow H + H_2O \quad \text{(R14)}$$

However, when 22.1 mol % of water was added to the feedstock at a higher temperature, water attends the reaction mainly via reactions R16r, R20r, and R22

$$CH_2(S) + H_2O \rightarrow CH_3 + OH \quad \text{(R16r)}$$

$$C_2H + H_2O \rightarrow C_2H_2 + OH \quad \text{(R20r)}$$

$$CHCO + H_2O \rightarrow CH_2CO + OH \quad \text{(R22)}$$

where $CH_2(S)$ represents singlet methylene; R16r and R20r represent the reverse reactions of R16 and R20, respectively.

The reaction of hydrogen is the most complicated. Generally, it is the competition between reactions R4 and R14. However, when 22.1 mol % of water was added to the feedstock at a higher temperature, the reaction rates of reactions 37 and 38 almost identically increase but towards different directions

$$CHCOH + H \rightarrow CHCO + H_2 \quad \text{(R37)}$$

$$CHCO + H_2 \rightarrow CH_2CO + H \quad \text{(R38)}$$

This can explain why the apparent conversion of hydrogen is low.

In combination with all fundamental reactions, the overall reaction includes the dry reforming (R1), steam reforming (R2), WGS reaction (R3), and the pyrolysis of methane to produce higher hydrocarbons

$$2CH_4 + \rightarrow C_2H_6 + H_2 \quad \text{(R44)}$$

$$2CH_4 + \rightarrow C_2H_4 + 2H_2 \quad \text{(R45)}$$

$$2CH_4 + \rightarrow C_2H_2 + 3H_2 \quad \text{(R46)}$$

$$CH_4 + \rightarrow C + 2H_2 \quad \text{(R47)}$$

where C represents all species above C_2, including PAH and solid carbon. Then, CH_4 and CO_2 conversions under 1500 °C regarding different reactions can be calculated from the mass balance simulated by kinetics, as shown in Table 2. From these results, we can find that both CH_4 and CO_2 conversions

https://doi.org/10.1021/acs.iecr.2c01680
Ind. Eng. Chem. Res. XXXX, XXX, XXX−XXX

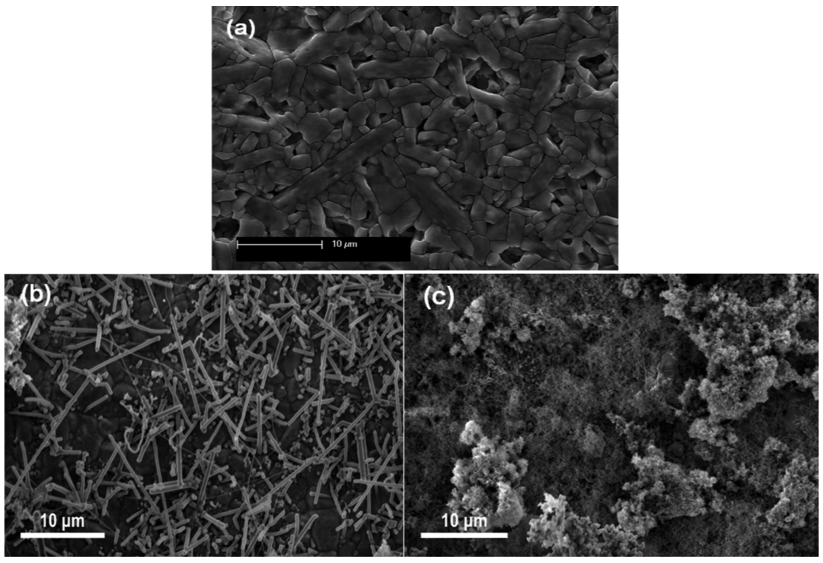

Figure 6. SEM image of the SiC wafer surface placed (a) outside, (b) on the top, and (c) in the middle of reactor's heating zone after 30 min of the reaction at 1500 °C at the flow of 2500 mL/min with a water content of 11.1 mol % ($F_{11.1}T_{1500}R_{2500}t_{30}$).

increase with the reaction temperature but decline with the water addition, except that the methane conversion increases with water addition when the flow rate is retained at 5000 mL/min. The kinetic simulation perfectly matches the experimental results and follows the same trend as the thermodynamic simulation results.

If one look at individual reactions, steam reforming does not occur within all tested conditions based on the kinetic modeling, as shown in Table 2. The dry reforming rate increases with the temperature and water addition; productions of ethane, ethylene, and higher hydrocarbons are at a low level which is almost within the experimental error, and the production of acetylene is quite high with a linear response to water addition depending on the flow rates. In the case of CO_2, the dry reforming ratio increases, and the reverse WGS reaction ratio decreases with water addition, which is understandable as the presence of water inhibits the reverse WGS reaction.[35]

5.5. Carbon Deposits on Internal Reactor Surfaces. Formation of carbon during the thermal upgrading causes a serious problem due to the buildup of carbon on internal reactor surfaces. Such deposition can cause a significant drop in the heat transfer that may lead to a local overheating or underheating of reactor zones, which has been confirmed by the time-on-steam conversion of the gas mixture with a water content of 5.04 mol % reacting at 1500 °C under the flow of 2500 mL/min from 10 to 240 min ($F_5T_{1500}R_{2500}t_{10}-F_5T_{1500}R_{2500}t_{240}$), as shown in Table S1 and Figure S3. This is caused the conversion reaching a peak and then steadily declining on time, which is the so-called transient phenomena. In that case, the simulation will have deviation as the heat transferring rate between the furnace and the gas stream inside the reactor changes due to the carbon deposition on the reactor wall. When the thermal upgrading of the biosyngas is performed, several strategies may be applied to deal with possible carbon formation and, thus, to minimize the transient phenomena on conversions. For example, the solid carbon can be periodically removed from the reactor and utilized in some other application. It can alternatively be periodically burned or gasified,[34] or its formation can be minimized by choosing a specific reaction condition, possibly with a controlled amount of steam presented in the system.

Figure 6 shows SEM images of wafer surfaces placed on the top (Figure 6b) and in the middle (Figure 6c) of the reactor heating zone, respectively, in comparison with the wafer outside the heating zone (Figure 6a). The corresponding wafers were analyzed by EDX analysis and Raman spectroscopy. Raman spectra are presented in Figure 7.

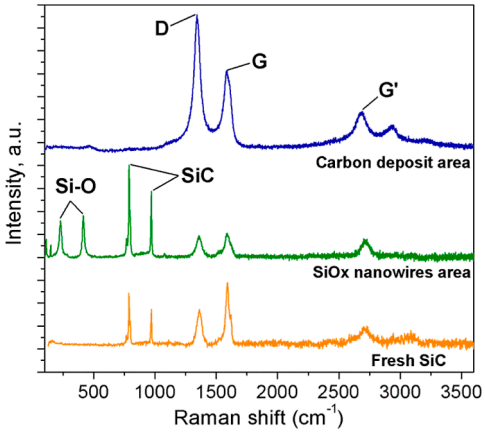

Figure 7. Raman spectra of SiC wafers placed in the middle of reactor zone (top) and on the top of heating zone (middle) after 30 min of the reaction at 1500 °C at the flow of 2500 mL/min with a water content of 11.1 mol % ($F_{11.1}T_{1500}R_{2500}t_{30}$), and a reference SiC wafer that was not exposed to the reaction environment (bottom).

Only the structure of α-SiC is found in Figure 6a, and a microsized species with a needle-like structure appears in Figure 6b. Raman spectra collected from the same area show peaks corresponding to Si−O and SiC. D and G bands are characteristics of the carbon formed and are also observed (SiO_x nanowires area data line, Figure 7), where D represents the vibrations out-of-plane attributed to the presence of structural defects, and G represents in-plane vibrations of SP^2-bonded carbon atoms of the graphene structure in Raman spectra. The silica structure with peaks detected at 230 and

https://doi.org/10.1021/acs.iecr.2c01680
Ind. Eng. Chem. Res. XXXX, XXX, XXX−XXX

414 cm^{-1} is attributed to cristobalite.[36] D and G bands characterizing the carbon deposits are observed at 1350 and 1580 cm^{-1}, respectively. Based on these observations, it is likely that the reactor material (SiC) undergoes a chemical reaction with the oxygen-containing species, possibly formed by the decomposition of CO_2 or H_2O. The overall reaction (reaction R48) includes the formation of SiO_2 and carbon. Formed SiO_2 precipitates on the reactor walls and forms needle-like microdomains, while carbon is carried away by the gas stream and precipitates further.

$$SiC + 2O \rightarrow SiO_2 + C \quad (R48)$$

The heated reactor zone represented by the SEM image in Figure 6c is significantly different from what was observed for the upper part of the reactor, and so does the corresponding Raman spectrum (Figure 7). The Raman spectrum from this zone shows exclusive peaks corresponding to carbon, possibly due to a low penetration depth of the laser excitation source used. Considering the relative intensity of the carbon bands (D, G) and in line with the previous work,[36] it can be concluded that carbon formed has a disordered, amorphous structure of a low density.

The combination of the results obtained from the top and the middle of the reactor hot zone allows us to speculate that the SiO_2 nanowires may act as a support to anchor the carbon formed during the reforming under the condition where the temperature is high enough to render the reaction between the reactor surface and oxygen source. At the same time, the SiO_2 nanowires enlarge the contact surface area between the reactor wall and the gas phase, which may consequently influence the surface reactions.

It is noted that the carbon deposition mechanism has been studied by this team in previous researches.[21,22,37,38] In this paper, we only concentrate on the effects of reaction parameters on carbon deposition rather than on the carbon deposition mechanism itself. Moreover, the silicon carbide wafers were believed to only affect the temperature distribution versus radius and the intersection area of the reactor, thereafter affecting the actual reaction temperature profile and the residence time of the reactants in the reaction zone instead of the reaction mechanism.[28,29,34]

6. CONCLUSIONS

Thermal processing to upgrade biosyngas was studied with an aim to convert the present CH_4 to H_2 and CO. In this approach a heat treatment promoting the noncatalytic thermal upgrading reactions are applied on the producer gas at conditions where full equilibration is not obtained. The reaction parameters such as the reaction temperature, the amount of added water, and residence time have been investigated, and their influences on conversions and productions of relevant components in the gas mixture were discussed. Obtained results are also discussed in the light of thermodynamic prediction and kinetic simulation. The detailed reaction mechanism is investigated as based on the simulation of the experimental results. The CO_2 conversion for the feedstock with water addition of 44.26 mol % at 1500 °C and 2500 mL/min was found at the similar level with the thermodynamic equilibrium value. The formation of carbon was proved to be caused by the methane pyrolysis, and the water addition can be applied to restrain the carbon formation. The main reaction pathways involve dry reforming of methane and reverse WGS reactions, while the steam reforming does not occur within all tested conditions. The dry reforming rate increases with the temperature and water addition. Water addition was proved to have benefit in reducing the reverse WGS reaction ratio.

A tubular reactor incorporating an electric furnace was operated for the thermal upgrading of biosyngas. The furnace provides a more effective and well-controlled heating method, which responds to the rapid changes in temperature to maintain the reaction at a steady state. The temperature profile was measured, and the furnace was evaluated by different reaction feedstock and conditions.

Experimental data show that a considerable enrichment of the producer gas with CO and H_2 occurs at a high temperature and a relatively long residence time. Under these conditions, the carbon formed in the reactor may represent a serious drawback of the novel concept. Several strategies are proposed to deal with the carbon formation; however, a significant lowering of the reaction temperature would require the use of a catalyst. In the last section, the carbon formed during the thermal upgrading is characterized, and its properties depending on the position within the reactor are described by SEM and Raman spectroscopy. The characterization results suggest a possible degradation of the reactor material (SiC) at the reaction conditions due to an interaction of SiC with the oxygen species present.

■ ASSOCIATED CONTENT

Supporting Information

The Supporting Information is available free of charge at https://pubs.acs.org/doi/10.1021/acs.iecr.2c01680.

Furnace controlling, biomass gasification gas thermal processing results, and kinetic simulation (PDF)

■ AUTHOR INFORMATION

Corresponding Authors

Chao'en Li − *CSIRO Energy, Victoria 3169, Australia*; orcid.org/0000-0003-4233-3172; Phone: +61 3 95458335; Email: Chaoen.Li@csiro.au

Woo Jin Lee − *CSIRO Energy, Victoria 3169, Australia*; Phone: +61 3 95458375; Email: Woojin.Lee@csiro.au

Jim Patel − *CSIRO Energy, Victoria 3169, Australia*; Phone: +61 3 95458356; Email: Jim.Patel@csiro.au

Authors

Svatopluk Chytil − *Department of Process Technology—Kinetics and Catalysis, SINTEF Industry, N-7465 Trondheim, Norway*; Present Address: Quantafuel ASA, Lilleakerveien 2C, 0283 Oslo, Norway

Rune Lødeng − *Department of Process Technology—Kinetics and Catalysis, SINTEF Industry, N-7465 Trondheim, Norway*

Anders Holmen − *Department of Chemical Engineering, Norwegian University of Science and Technology (NTNU), N-7491 Trondheim, Norway*; orcid.org/0000-0001-7967-9711

Edd A. Blekkan − *Department of Chemical Engineering, Norwegian University of Science and Technology (NTNU), N-7491 Trondheim, Norway*; orcid.org/0000-0002-3620-3884

Nick Burke − *CSIRO Energy, Victoria 3169, Australia*; Present Address: Carbon Innovation & Earth Resources Policy and Programs, Department of Jobs, Precincts and

https://doi.org/10.1021/acs.iecr.2c01680
Ind. Eng. Chem. Res. XXXX, XXX, XXX−XXX

Regions, 1 Spring Street, Melbourne, Victoria 3000, Australia.

Complete contact information is available at: https://pubs.acs.org/10.1021/acs.iecr.2c01680

Notes

The authors declare no competing financial interest.

■ ACKNOWLEDGMENTS

The financial support by Chevron for the furnace design and commission is gratefully acknowledged. The authors thank Dr Karl Gerdes of Chevron Energy Technology for his support; Merrill Wilson and James Cutts of Ceramatec Inc. for providing ceramic materials; Dr Steven Wang for his important contribution in performing the experiments and programing of LabVIEW; Aishwarya Swaminathan for attending the experiments; and Prof. Peter Glarborg (Technical University of Denmark) for supplying a CHEMKIN formatted version of the combustion mechanism used in kinetic simulations. S.C. thanks the financial support from Norwegian Research Council, the Gas Technology Centre at NTNU/SINTEF, Statoil, Vista, NTNU, and SINTEF for his study in CSIRO, Australia.

■ NOMENCLATURE

CFD	computational fluid dynamic modeling
$Covt_i$	conversions of component i
D	out-of-plane vibrations in Raman spectrum attributed to the presence of structural defects
ΔH°_{298}	enthalpy changes at room temperature
EDX	energy-dispersive X-ray
$F_{11.1}T_{1500}R_{2500}t_{30}$	experiment with water addition = 11.1 mol %, at the temperature of 1500 °C, under the flow rate of 2500 mL/min, and when the reaction time = 30 min
$F_{i,\mathrm{in}}$	molar flow of compound i in the feed
$F_{i,\mathrm{out}}$	molar flow of compound i in the product
G	in-plane vibrations of SP^2 bonded carbon atoms of graphene structure in Raman spectrum
$L_{36.1}$	at the position of 36.1 cm from the inlet of the reactor
N_i	the stoichiometric coefficients of component i in the stoichiometrically balanced reaction equation
PAH	polycyclic aromatic hydrocarbon
$Prod_i$	production of component i
SEM	scanning electron microscopy

■ REFERENCES

(1) Carlu, E.; Truong, T.; Kundevski, M. *Biogas Opportunities for Australia*; ENEA Consulting, 2019; pp 1−53.
(2) Buss, J.; Mansuy, N.; Madrali, S. De-Risking Wood-Based Bioenergy Development in Remote and Indigenous Communities in Canada. *Energies* **2021**, *14*, 2603.
(3) IEA. Outlook for biogas and biomethane—prospects for organic growth. *World Energy Outlook Special Report*, 2020; pp 1−93.
(4) Lepage, T.; et al. Biomass-to-hydrogen: A review of main routes production, processes evaluation and techno-economical assessment. *Biomass Bioenergy* **2021**, *144*, 105920.
(5) Rabou, L. P. L. M.; et al. Tar in Biomass Producer Gas, the Energy research Centre of The Netherlands (ECN) Experience: An Enduring Challenge. *Energy Fuels* **2009**, *23*, 6189−6198.
(6) Sadaka, S. Gasification, Producer Gas and Syngas. *Agriculture and Natural Resources*; University of Arkansas Printing Services, 2017; pp 1−8.
(7) Torres, W.; Pansare, S. S.; Goodwin, J. G. Hot Gas Removal of Tars, Ammonia, and Hydrogen Sulfide from Biomass Gasification Gas. *Catal. Rev.* **2007**, *49*, 407−456.
(8) Makwana, H. V.; et al. *Strategies for Producer Gas Cleaning in Biomass Gasification: A Review*; Springer Singapore: Singapore, 2018.
(9) Valin, S.; et al. Upgrading biomass pyrolysis gas by conversion of methane at high temperature: Experiments and modelling. *Fuel* **2009**, *88*, 834−842.
(10) Wangen, E. S.; Osatiashtiani, A.; Blekkan, E. Reforming of Syngas from Biomass Gasification: Deactivation by Tar and Potassium Species. *Top. Catal.* **2011**, *54*, 960−966.
(11) Haryanto, A.; et al. Upgrading of syngas derived from biomass gasification: A thermodynamic analysis. *Biomass Bioenergy* **2009**, *33*, 882−889.
(12) Lee, W. J.; Li, C.; Patel, J. Upgrading of Bio-Syngas via Steam-CO2 Reforming Using Rh/Alumina Monolith Catalysts. *Catalysts* **2021**, *11*, 180.
(13) Lavoie, J.-M. Review on dry reforming of methane, a potentially more environmentally-friendly approach to the increasing natural gas exploitation. *Front. Chem.* **2014**, *2*, 81.
(14) Chen, D.; et al. Deactivation during carbon dioxide reforming of methane over Ni catalyst: microkinetic analysis. *Chem. Eng. Sci.* **2001**, *56*, 1371−1379.
(15) Zhao, X.; et al. Biogas Reforming to Syngas: A Review. *iScience* **2020**, *23*, 101082.
(16) Arora, S.; Prasad, R. An overview on dry reforming of methane: strategies to reduce carbonaceous deactivation of catalysts. *RSC Adv.* **2016**, *6*, 108668−108688.
(17) Wittich, K.; et al. Catalytic Dry Reforming of Methane: Insights from Model Systems. *ChemCatChem* **2020**, *12*, 2130−2147.
(18) Torres, M. T. Non-Catalytic Reforming of Biogas in Porous Media Combustion. *Anaerobic Digestion*; Banu, J. R., Ed.; IntechOpen, 2019; p 1−15.
(19) Espinoza, L.; et al. Syngas production by non-catalytic reforming of biogas with steam addition under filtration combustion mode. *Int. J. Hydrogen Energy* **2018**, *43*, 15693−15702.
(20) Dufour, A.; et al. Mechanisms and Kinetics of Methane Thermal Conversion in a Syngas. *Ind. Eng. Chem. Res.* **2009**, *48*, 6564−6572.
(21) Lee, W. J.; et al. The growth and morphology of core/shell heterostructured conical carbon fibers. *Carbon* **2011**, *49*, 2735−2741.
(22) Lee, W. J.; et al. Is the structure of anisotropic pyrolytic carbon a consequence of growth by the Volmer-Weber island growth mechanism? *Carbon* **2012**, *50*, 4773−4780.
(23) Cunha, A. F.; et al. Catalytic bi-reforming of methane for carbon dioxide ennoblement. *Energy Rep.* **2020**, *6*, 74−79.
(24) Jakobsen, J. G.; et al. Steam and CO2 reforming of methane over a Ru/ZrO2 catalyst. *Appl. Catal., A* **2010**, *377*, 158−166.
(25) Roy, P. S.; et al. CO2 conversion to syngas through the steam-biogas reforming process. *J. CO2 Util.* **2018**, *25*, 275−282.
(26) Bradford, M. C. J.; Vannice, M. A. CO2 Reforming of CH4. *Catal. Rev.* **1999**, *41*, 1−42.
(27) Von Storch, H.; Becker-Hardt, S.; Sattler, C. (Solar) Mixed Reforming of Methane: Potential and Limits in Utilizing CO2 as Feedstock for Syngas Production—A Thermodynamic Analysis. *Energies* **2018**, *11*, 2537.
(28) Lee, W. J.; et al. Microstructure formation on exposure of silicon carbide surfaces to the partial oxidation of methane. *Catal. Today* **2011**, *178*, 85−97.
(29) Wang, S.; et al. The pyrolysis of natural gas: A study of carbon deposition and the suitability of reactor materials. *AIChE J.* **2019**, *65*, 1035−1046.

https://doi.org/10.1021/acs.iecr.2c01680
Ind. Eng. Chem. Res. XXXX, XXX, XXX−XXX

(30) Skjøth-Rasmussen, M. S.; et al. Formation of polycyclic aromatic hydrocarbons and soot in fuel-rich oxidation of methane in a laminar flow reactor. *Combust. Flame* **2004**, *136*, 91−128.
(31) Li, C. e.; et al. The non-catalytic partial oxidation of methane in a flow tube reactor using indirect induction heating − An experimental and kinetic modelling study. *Chem. Eng. Sci.* **2018**, *187*, 189−199.
(32) Choudhary, V. R.; Mondal, K. C. CO2 reforming of methane combined with steam reforming or partial oxidation of methane to syngas over NdCoO3 perovskite-type mixed metal-oxide catalyst. *Appl. Energy* **2006**, *83*, 1024−1032.
(33) Demirel, E.; Ayas, N. Thermodynamic modeling of the water-gas shift reaction in supercritical water for hydrogen production. *Theor. Found. Chem. Eng.* **2017**, *51*, 76−87.
(34) Wang, S.; et al. Pyrolysis of Natural Gas: Effects of Process Variables and Reactor Materials on the Product Gas Composition. *Chem. Eng. Technol.* **2019**, *42*, 690−698.
(35) Wolf, A.; Jess, A.; Kern, C. Syngas Production via Reverse Water-Gas Shift Reaction over a Ni-Al2O3 Catalyst: Catalyst Stability, Reaction Kinetics, and Modeling. *Chem. Eng. Technol.* **2016**, *39*, 1040−1048.
(36) Lee, W. J.; et al. Heat treatment of 6H-SiC under different gaseous environments. *Ceram. Int.* **2014**, *40*, 4149−4154.
(37) Lee, W. J.; et al. The growth of 3D carbon fiber lattices based on silicon oxide micro-wires. *Carbon* **2011**, *49*, 1167−1172.
(38) Wan, W.; et al. The thickening of carbon fibers via a 3D island growth mechanism: New insights from a theoretical and experimental study. *Carbon* **2019**, *152*, 851−854.

https://doi.org/10.1021/acs.iecr.2c01680
Ind. Eng. Chem. Res. XXXX, XXX, XXX−XXX